NMR Structural Studies of the Ionizing Radiation Adduct 7-Hydro-8-oxodeoxyguanosine (8-oxo-7*H*-dG) opposite Deoxyadenosine in a DNA Duplex. 8-Oxo-7*H*-dG(*syn*)·dA(*anti*) Alignment at Lesion Site†

Michael Kouchakdjian,‡ Veeraiah Bodepudi,§ Shinya Shibutani,§ Moises Eisenberg,§ Francis Johnson,§ Arthur P. Grollman,*,§ and Dinshaw J. Patel*,‡

Department of Biochemistry and Molecular Biophysics, College of Physicians and Surgeons, Columbia University, New York, New York 10032, and Department of Pharmacological Sciences, State University of New York at Stony Brook, Stony Brook, New York 11794

Received July 26, 1990; Revised Manuscript Received October 1, 1990

ABSTRACT: Proton NMR studies are reported on the complementary d(C1-C2-A3-C4-T5-A6-oxo-G7-T8-C9-A10-C11-C12)·d(G13-G14-T15-G16-A17-A18-T19-A20-G21-T22-G23-G24) dodecanucleotide duplex (designated 8-oxo-7*H*-dG·dA 12-mer), which contains a centrally located 7-hydro-8-oxodeoxyguanosine (8-oxo-7*H*-dG) residue, a group commonly found in DNA that has been exposed to ionizing radiation or oxidizing free radicals. From the NMR spectra it can be deduced that this moiety exists as two tautomers, or gives rise to two DNA conformations, that are in equilibrium and that exchange slowly. The present study focuses on the major component of the equilibrium that originates in the 6,8-dioxo tautomer of 8-oxo-7*H*-dG. We have assigned the exchangeable NH1, NH7, and NH_2-2 base protons located on the Watson–Crick and Hoogsteen edges of 8-oxo-7*H*-dG7 in the 8-oxo-7*H*-dG·dA 12-mer duplex, using an analysis of one- and two-dimensional nuclear Overhauser enhancement (NOE) data in H_2O solution. The observed NOEs derived from the NH7 proton of 8-oxo-7*H*-dG7 to the H2 and NH_2-6 protons of dA18 establish an 8-oxo-7*H*-dG7(*syn*)·dA18(*anti*) alignment at the lesion site in the 8-oxo-7*H*-dG·dA 12-mer duplex in solution. This alignment, which places the 8-oxo group in the minor groove, was further characterized by an analysis of the NOESY spectrum of the 8-oxo-7*H*-dG·dA 12-mer duplex in D_2O solution. We were able to detect a set of intra- and interstrand NOEs between protons (exchangeable and nonexchangeable) on adjacent residues in the d(A6-oxo-G7-T8)·d(A17-A18-T19) trinucleotide segment centered about the lesion site that establishes stacking of the oxo-dG7(*syn*)·dA(*anti*) pair between stable Watson–Crick dA6·dT19 and dT8·dA17 base pairs with minimal perturbation of the helix. Thus, both strands of the 8-oxo-7*H*-dG·dA 12-mer duplex adopt right-handed conformations at and adjacent to the lesion site, the unmodified bases adopt anti glycosidic torsion angles, and the bases are stacked into the helix. The energy-minimized conformation of the central d(A6-oxo-G7-T8)·d(A17-A18-T19) segment requires that the 8-oxo-7*H*-dG7(*syn*)·dA18(*anti*) alignment be stabilized by two hydrogen bonds from NH7 and O6 of 8-oxo-7*H*-dG7(*syn*) to N1 and NH_2-6 of dA18(*anti*), respectively, at the lesion site. The proposed hydrogen-bond formation involving the Hoogsteen edge of 8-oxo-7*H*-dG is consistent with the 12.57 ppm downfield shift of the NH7 proton (hydrogen-bonded) and the 10.54 ppm upfield shift of the NH1 proton (not hydrogen-bonded) of 8-oxo-7*H*-dG(*syn*) in the 8-oxo-7*H*-dG·dA 12-mer duplex. Our structural studies demonstrate that 8-oxo-7*H*-dG(*syn*)·dA(*anti*) forms a stable pair in the interior of the helix, providing a basis for the observed incorporation of dA opposite 8-oxo-7*H*-dG when readthrough occurs past this oxidized nucleoside base.

The attack of reactive oxygen species on DNA represents an important mechanism by which exogenous and endogenous agents may inflict damage on cells. Oxygen-derived free radicals, produced by ionizing radiation (Ward, 1988; Hutterman et al., 1978) or arising from cellular metabolism (Cerutti, 1985; DiGuiseppi & Fridovich, 1984) generate apurinic/apyrimidinic sites or base modifications in DNA; both types of lesions may have mutagenic and carcinogenic effects (Breimer, 1988).

Deoxyguanosine residues in DNA are hydroxylated by oxygen radicals at the C-8 position to form 7-hydro-8-oxo-2′-deoxyguanosine (Kasai & Nishimura, 1984a–c; Dizdaroglu, 1985). In its monomeric form, this modified base adopts several tautomeric structures (Aida & Nishimura, 1987); the 6,8-dioxo species (designated 8-oxo-7*H*-dG) predominates under physiological conditions (Culp et al., 1989).

Recent studies in our laboratory have established that translesional synthesis can proceed past 8-oxo-7*H*-dG in primed template reactions catalyzed by DNA polymerase, in which case dA and/or dC is inserted opposite the lesion. The 8-oxo-7*H*-dG·dA pair is readily extended by DNA polymerase and does not appear to be subject to the editing function of this enzyme (Shibutani et al., 1991).

In an attempt to correlate the structural and base-pairing relationships of 8-substituted purines in DNA with observed biological properties, we have used NMR studies coupled with energy minimization techniques to characterize their role in the three-dimensional structure of DNA in solution (Norman et al., 1989). In this paper, we report experimental data that establish the structural relationships of an 8-oxo-7*H*-dG residue, **1**, located opposite dA and embedded in a dodecanucleotide duplex, **2**.

† This research was supported in part by a Columbia University Faculty Start-up grant and in part by NIH Grant CA-46533 to D.J.P. and by NIH Grants ES-04068 and CA-17395 to A.P.G., M.E., and F.J. NMR studies were conducted on instruments purchased with funds provided by the Robert Woods Johnson Jr. Charitable Trust and the Matheson Foundation.

‡ Columbia University.

§ SUNY at Stony Brook.

0006-2960/91/0430-1403$02.50/0

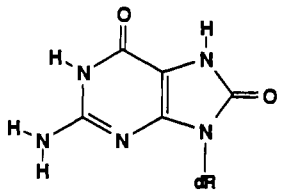

1

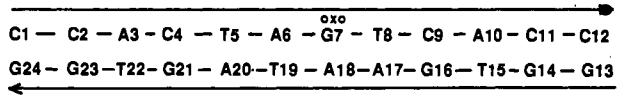

2

Experimental Procedures

Synthesis and Purification of 8-Oxo-dG. The protected phosphoramidite of 7-hydro-8-oxo-2′-deoxyguanosine required for the synthesis of the oligomers (Bodepudi et al., 1991) was synthesized from 8-(benzyloxy)deoxyguanosine (Lin et al., 1985) by using standard methods. Acylation of the latter compound by isobutyric anhydride via the transient protection method (Ti et al., 1982) led to the N^2-isobutyryl derivative, which on catalytic hydrogenation gave N^2-isobutyryl-8-oxo-2′-deoxyguanosine. Treatment with 4,4′-dimethoxytrityl (DMT) chloride in the presence of pyridine yielded the 5′-DMT derivative in excellent yield. Further treatment with 2-cyanoethyl *N*-diisopropylaminochlorophosphite, using Et_3N to remove HCl, then afforded the required phosphoramidite. Kuchino et al. (1987) incorporated a 7-hydro-8-oxo-2′-deoxyguanosine residue into oligomeric DNA by using a protected form (8-methoxy derivative) of the 7-hydro-8-oxo group, followed by a deprotection sequence. We did not consider protection of the 8-oxygen atom necessary during DNA synthesis since it is part of a urea system and like the 2-oxo group of thymidine should require no protection. In any event, no interference in DNA synthesis was observed. It did, however, prove necessary during the deprotection step of oligomer synthesis to include mercaptoethanol to inhibit oxidative degradation (Shibutani et al., 1990) at the 7-hydro-8-oxo-dG site, which can lead to chain cleavage.

Oligonucleotide Synthesis and Purification. Oligodeoxynucleotides, including those containing 8-oxo-dG, were prepared by solid-state synthesis on a Du Pont Coder 300 automated DNA synthesizer and isolated as previously reported (Takeshita et al., 1987) except that the 7-hydro-8-oxo-dG-modified oligomer was removed from the resin support by means of concentrated ammonia containing 0.1 M 2-mercaptoethanol at 55 °C for 16 h. These oligonucleotides were purified twice on a reverse-phase column, μBondapak C18 (0.78 × 30 cm, Waters) and eluted with a linear gradient of 0.05 M triethylamine acetate (pH 7.0) containing 10–15% acetonitrile over 60 min. After each oligonucleotide was labeled with ^{32}P at the 5′ terminus (Maniatis et al., 1982), the principal product migrated as a single band when subjected to electrophoresis on a 20% polyacrylamide gel in the presence of 7 M urea. No degradation product was detected after incubating the 8-oxo-7*H*-dG-modified oligonucleotide in 100 mM Tris-HCl buffer (pH 7.0 or 8.0) at 56 °C for 2 h, as in the annealing conditions, or at 37 °C for 5 days.

Sample Preparation. The addition of the 8-oxo-7*H*-dG7-containing strand to the unmodified strand to generate the complementary 8-oxo-7*H*-dG·dA 12-mer duplex was monitored by following the intensities of resolved base proton markers on each strand in D_2O at 60 °C. The NMR spectra were run on 400 A_{260} units of the 8-oxo-7*H*-dG·dA 12-mer in 0.1 M NaCl containing 10 mM phosphate and 1 mM EDTA in either 100% D_2O or 90% H_2O/10% D_2O (v/v) at 9 °C. The pH values in D_2O are uncorrected pH meter readings.

NMR Experiments. One- and two-dimensional proton NMR data sets were collected on a Bruker AM 500 spectrometer and are referenced relative to external 3-(trimethylsilyl)propionate-*2,2,3,3-d*$_4$ (TSP). The phosphorus spectrum was referenced relative to external trimethyl phosphate (TMP).

Two-dimensional proton NOESY experiments in H_2O were performed with a jump and return (90_y, τ, 90_{-y}) detection pulse. Two-dimensional proton NOESY spectra in D_2O were recorded at mixing times of 50, 80, and 250 ms. The residual HOD resonance in this experiment was presaturated by using the decoupler channel. Pulse sequences, data accumulation, and processing parameters for all NMR experiments in both H_2O and D_2O have been described previously (Kouchakdjian et al., 1989, 1990). Data sets were processed by using FTNMR software on a VAX 6310 minicomputer.

Distance Constraints. The volume integrals of the resolved cross peaks were measured at mixing times of 50, 80, and 250 ms in NOESY spectra of the 8-oxo-7*H*-dG·dA 12-mer duplex in D_2O solution. Interproton distances were estimated on the basis of the inverse sixth power distance dependence of the intensity of the NOE cross peaks and measured relative to the volume integrals of the deoxycytidine H5–H6 cross peaks corresponding to the fixed 2.45-Å distance. The estimated distances were given boundaries ranging from 0.6 to 1.0 Å for NOESY data collected at mixing times of 50 and 80 ms and boundaries ranging from 0.8 to 1.0 Å for NOESY data collected at a mixing time of 250 ms. These relatively wide boundaries reflect the inherent limitations of the two-spin approximation and the neglect of possible differential local motion for estimating interproton distances.

Energy Minimization. The starting structure was a standard B-form DNA duplex with the sequence referenced above. It was built with the assistance of the computer program BioGraf (BioDesign, Pasadena) on an Alliant FX-1 minisupercomputer attached to an Evans & Sutherland PS-390 graphics workstation. The H8 hydrogen of the dG7 residue was replaced by an oxygen double-bonded to C8, and a hydrogen was linked to N7. The glycosidic bond on dG7 was set to the syn conformation in accordance with the NMR data as reported under Results.

Energy minimization was conducted on the structure by using the computer program XPLOR (Brunger, 1988) running on a Convex C2-20 minisupercomputer. Five thousand steps of conjugate gradient minimization were applied with 151 distance restraints for hydrogen pairs as determined from the NOESY data set. These distance restraints were of the form of square well potentials with steep boundaries at the upper and lower bounds of the NOE-determined distances. In addition, the distances between N–H---N central hydrogen bonds of all base pairs other than the lesion site location were restrained as well to maintain Watson–Crick base pairing. Distances between hydrogen pairs of the final model were measured and compared with those deduced from the NMR experiments. The final total energy of the minimized structure was 131 kcal.

Results

The exchangeable proton (6.0–14.5 ppm), nonexchangeable proton (5.2–8.8 ppm), and phosphorus (−3.1 to −5.2 ppm) spectra of the 8-oxo-7*H*-dG·dA 12-mer duplex are plotted in Figure 1, panels A, B, and C, respectively. Both the narrow,

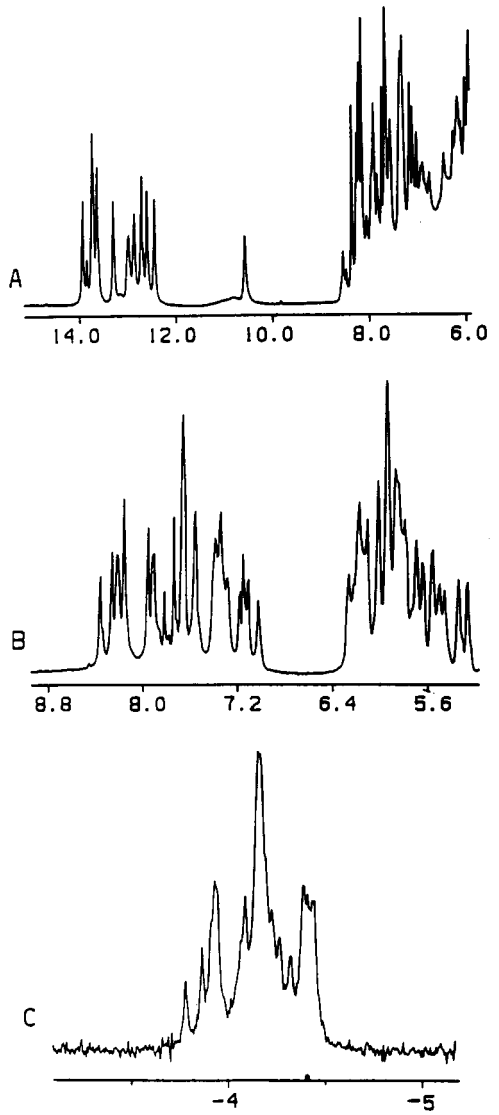

FIGURE 1: (A) Exchangeable proton spectrum (6.0–14.5 ppm), (B) nonexchangeable proton spectrum (5.2–8.8 ppm), and (C) proton decoupled phosphorus spectrum (−3.1 to −5.2 ppm) of the 8-oxo-7*H*-dG·dA 12-mer duplex in a buffer of 0.1 M NaCl, 10 mM phosphate, and 1 mM EDTA in H_2O, pH 6.1, at 9 °C.

well-resolved proton spectra (Figure 1A,B) are amenable to further characterization by two-dimensional NMR experiments. We detect minor resonances in the proton spectra (Figure 1A,B) indicative of a second component in slow equilibrium with the major form of the 8-oxo-7*H*-dG·dA 12-mer duplex. Our current efforts focus on the structural characterization of the major conformation.

Exchangeable Protons. The imino protons (12.4–13.9 ppm) along with the exchangeable proton at 10.54 ppm in the 8-oxo-7*H*-dG·dA 12-mer duplex (Figure 1A) have been assigned by analysis of two-dimensional NOESY and one-dimensional NOE experiments in H_2O solution. An expanded NOESY (mixing time 120 ms) contour plot exhibiting NOE cross peaks between the imino protons (10.0–14.0 ppm) and the base and amino protons (5.8–8.8 ppm) of the 8-oxo-7*H*-dG·dA 12-mer duplex in H_2O buffer, pH 6.1, at 9 °C is plotted in Figure 2. There are five internal dA·dT base pairs in the 8-oxo-7*H*-dG·dA 12-mer duplex, and we detect five strong cross peaks between thymidine imino protons and deoxyadenosine H2 protons (peaks A–E, Figure 2). The deoxyadenosine H2 protons at positions dA3, dA10, and dA17 (as well as dA18 at the 8-oxo-7*H*-dG7·dA18 lesion site) can be independently assigned by analysis of NOESY data in D_2O solution. This

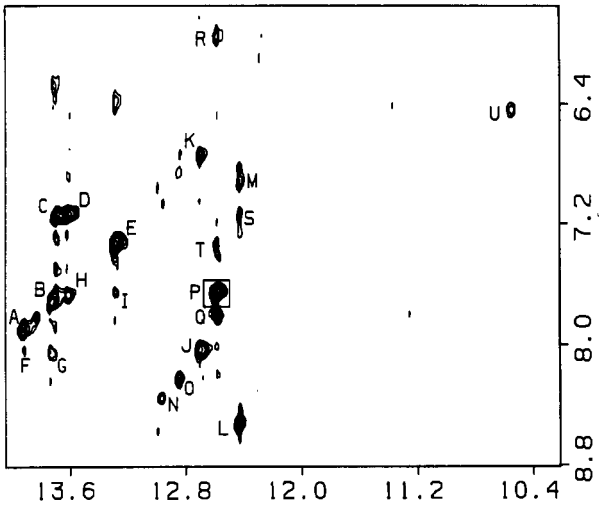

FIGURE 2: Expanded contour plot of the NOESY spectrum (mixing time 120 ms) of the 8-oxo-7*H*-dG·dA 12-mer duplex in a buffer of 0.1 M NaCl and 10 mM phosphate in H_2O, pH 6.1, at 9 °C, establishing distance connectivities between the imino protons (10.0–14.0 ppm) and the base and amino protons (5.8–8.8 ppm). The peaks A–U are assigned as follows: A, T22(NH3)–A3(H2); B, T15(NH3)–A10(H2); C, T5(NH3)–A20(H2); D, T8(NH3)–A17(H2); E, T19(NH3)–A6(H2); F, T22(NH3)–C4(NH_2b); G, T5(NH3)–C4(NH_2b); H, T8(NH3)–A18(H2); I, T19(NH3)–A18(H2); J, G21(NH1)–C4(NH_2b); K, G21(NH1)–C4(NH_2e); L, G16(NH1)–C9(NH_2b); M, G16(NH1)–C9(NH_2e); N, O, G14(NH3)/G23(NH3)–C11(NH_2b)/C2(NH_2b); P, oxo-G7(NH7)–A18(H2); Q, oxo-G7(NH7)–A18(NH_2b); R, oxo-G7(NH7)–A18(NH_2e); S, G16(NH1)–A17(H2); T, oxo-G7(NH7)–A6(H2); U, oxo-G7(NH1)–oxo-G7(NH_2b,e).

has permitted the assignment of the observed NOE cross peaks to the dA3·dT22 (peak A, Figure 2), dA10·dT15 (peak B, Figure 2), dT5·dA20 (peak C, Figure 2), dT8·dA17 (peak D, Figure 2), and dA6·dT19 (peak E, Figure 2) base pairs in the 8-oxo-7*H*-dG·dA 12-mer duplex.

There are six dG·dC base pairs in the 8-oxo-7*H*-dG·dA 12-mer duplex with dC4·dG21 and dC9·dG16 in the interior while the remaining dG·dC pairs are at the ends of the helix. We can assign the imino protons of the internal dG·dC pairs on the basis of observed NOEs across the dG·dC pair and to flanking dA·dT pairs. Thus, the imino proton of dG16 exhibits NOEs to the amino protons of dC9 (peaks L and M, Figure 2) within the dC9·dG16 pair and to the H2 proton of dA17 of the adjacent dT8·dA17 pair (peak S, Figure 2). The imino proton of dG21 exhibits NOEs to the amino protons of dC4 (peaks J and K, Figure 2) within the dC4·dG21 pair. The hydrogen-bonded amino proton of dC4 also exhibits NOEs to the imino proton of dT22 (peak F, Figure 2) of the adjacent dA3·dT22 pair in one direction and to the imino proton of dT5 (peak G, Figure 2) of the adjacent dT5·dA20 pair in the other direction. The imino proton resonances at 12.95 and 12.83 ppm exhibit weak NOEs to their hydrogen-bonded deoxycytidine amino protons (peaks N and O, respectively, Figure 2), so that we are unable to distinguish between assignments of these imino protons to the dC2·dG23 and dC11·dG14 base pairs, which are one position in from either end of the 8-oxo-7*H*-dG·dA 12-mer duplex. The imino protons of the terminal dG·dC pairs are not detected as narrow resonances in the one-dimensional NMR spectrum (Figure 1A) and are most likely broadened due to rapid exchange in the 8-oxo-7*H*-dG·dA 12-mer duplex in H_2O, pH 6.1, at 9 °C.

The exchangeable proton at 12.57 ppm exhibits a strong NOE to the H2 proton of dA18 (peak P, Figure 2), displays NOEs to a pair of amino protons (peaks Q and R, Figure 2) assigned to dA18, and has a weaker NOE to the H2 proton

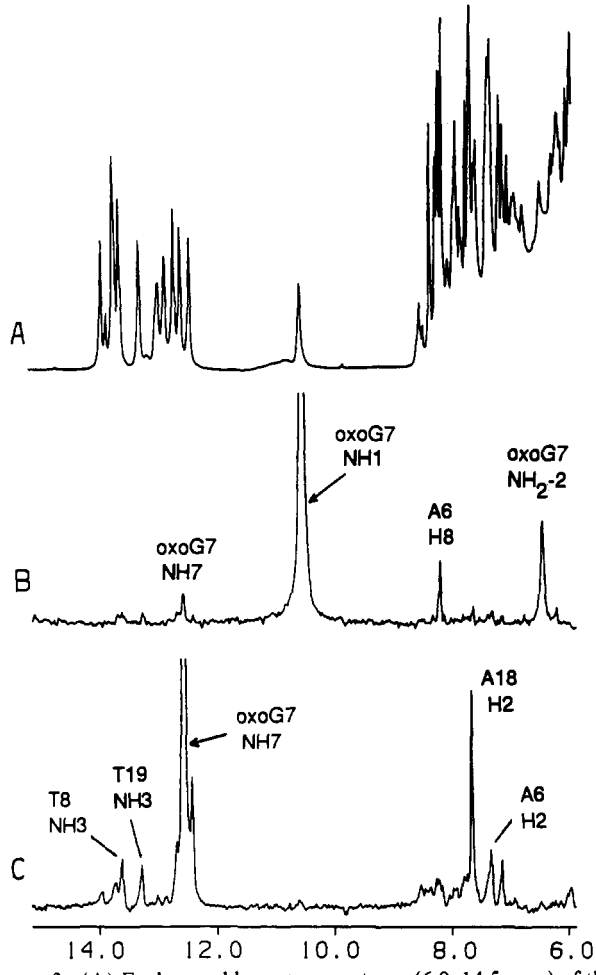

FIGURE 3: (A) Exchangeable proton spectrum (6.0–14.5 ppm) of the 8-oxo-7*H*-dG·dA 12-mer duplex in buffer of 0.1 M NaCl and 10 mM phosphate in H_2O, pH 6.1, at 9 °C. One-dimensional NOE difference spectra following 0.4-s saturation of (B) the 10.54 ppm resonance and (C) the 12.57 ppm resonance. The saturated resonance is designated by an arrow.

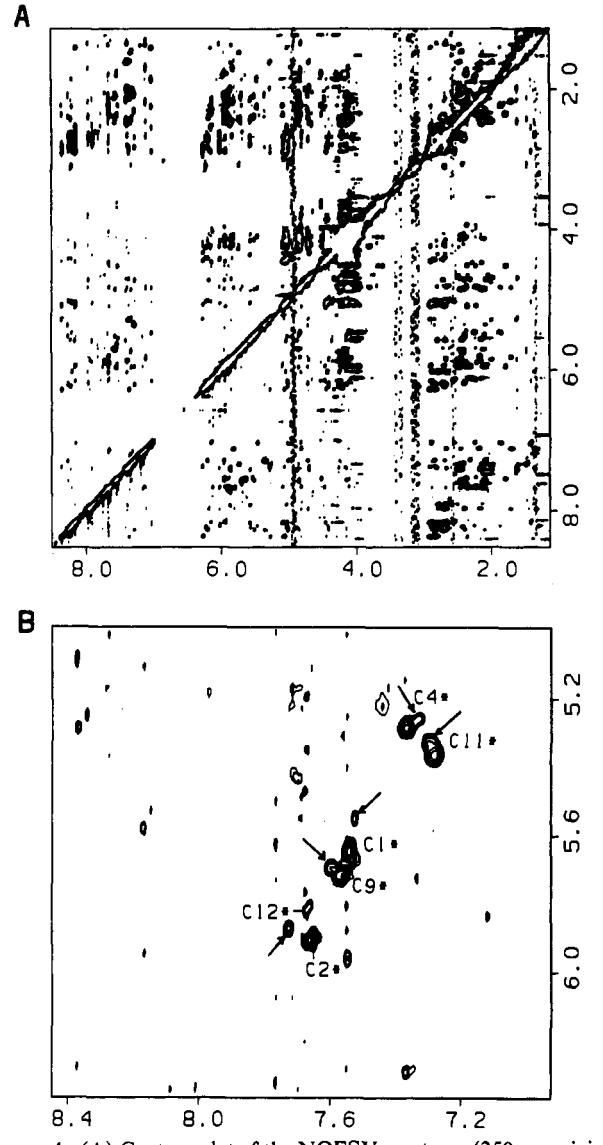

FIGURE 4: (A) Contour plot of the NOESY spectrum (250-ms mixing time) of the 8-oxo-7*H*-dG·dA 12-mer duplex in a buffer of 0.1 M NaCl and 10 mM phosphate in D_2O, pH 6.1, at 9 °C. (B) An expanded contour plot of the 50-ms mixing time NOESY spectrum correlating the base protons (6.9–8.4 ppm) with the sugar H1′ and cytidine H5 protons (5.0–6.4 ppm) in the 8-oxo-7*H*-dG·dA 12-mer duplex in a buffer of 0.1 M NaCl and 10 mM phosphate in D_2O, pH 6.1, at 9 °C. The deoxycytidine H6–H5 cross peaks of the predominant conformation are designated by asterisks, while those of the minor conformation are identified by arrows.

of dA6 (peak T, Figure 2) in the 8-oxo-7*H*-dG·dA 12-mer duplex. These data permit assignment of the 12.57 ppm resonance to the NH7 imino proton of 8-oxo-7*H*-dG7. These observed NOEs can exist only in a structure having an oxo-dG7(*syn*)·dA18(*anti*) alignment, which brings the NH7 of 8-oxo-7*H*-dG7 in close proximity to the H2 and NH_2-6 protons of dA18 at the lesion site. We also note that the H2 proton of A18 at the oxo-dG7·dA18 lesion site exhibits an NOE with the imino protons of adjacent dT8·dA17 (peak H, Figure 2) and dA6·dT19 (peak I, Figure 2) pairs in the 8-oxo-7*H*-dG·dA 12-mer duplex. We detect an NOE cross peak between the 10.54 and 6.45 ppm exchangeable resonances in the 120-ms mixing time NOESY spectrum of the 8-oxo-7*H*-dG·dA 12-mer duplex (peak U, Figure 2).

We have also undertaken one-dimensional NOE difference experiments following 0.4-s saturation of the 10.54 ppm exchangeable resonance in the 8-oxo-7*H*-dG·dA 12-mer duplex in H_2O buffer, pH 6.1, at 9 °C. The difference spectrum is plotted in Figure 3B. We detect a weak NOE to the 12.57 ppm resonance assigned to the NH7 imino proton of 8-oxo-7*H*-dG7, with the averaged amino exchangeable protons at 6.45 ppm, and to the 8.21 ppm H8 proton of A6 (Figure 3B). These results permit assignment of the 10.54 and 6.45 ppm exchangeable resonances to the NH1 imino proton and averaged NH_2-2 amino protons of 8-oxo-7*H*-dG7(*syn*), respectively, in the 8-oxo-7*H*-dG·dA 12-mer duplex. The one-dimensional NOE difference spectrum following saturation of the 12.57 ppm NH7 imino proton of 8-oxo-7*H*-dG7 is plotted in Figure 3C, and the observed NOEs confirm the assignments in the corresponding two-dimensional NOESY experiment (Figure 2). It is important to note that the 8-oxo-7*H*-dG7 base contains no nonexchangeable protons, and our ability to assign NH1 (10.54 ppm), NH7 (12.57 ppm), and NH_2-2 (6.45 ppm) exchangeable protons provides proton markers that are distributed throughout the 8-oxo-7*H*-dG7 ring system in the 8-oxo-7*H*-dG·dA 12-mer duplex.

The imino and amino exchangeable protons and the deoxyadenosine H2 proton chemical shifts in the 8-oxo-7*H*-dG·dA 12-mer duplex in H_2O buffer at 9 °C are listed in Table I.

Nonexchangeable Protons. The nonexchangeable protons have been assigned following analysis of the NOESY (250-ms mixing time) spectrum of the 8-oxo-7*H*-dG·dA 12-mer duplex in D_2O buffer, pH 6.1, at 9 °C (Figure 4A). Expanded duplicate contour plots that establish distance connectivities between the base protons (6.9–8.4 ppm) and the sugar H1′

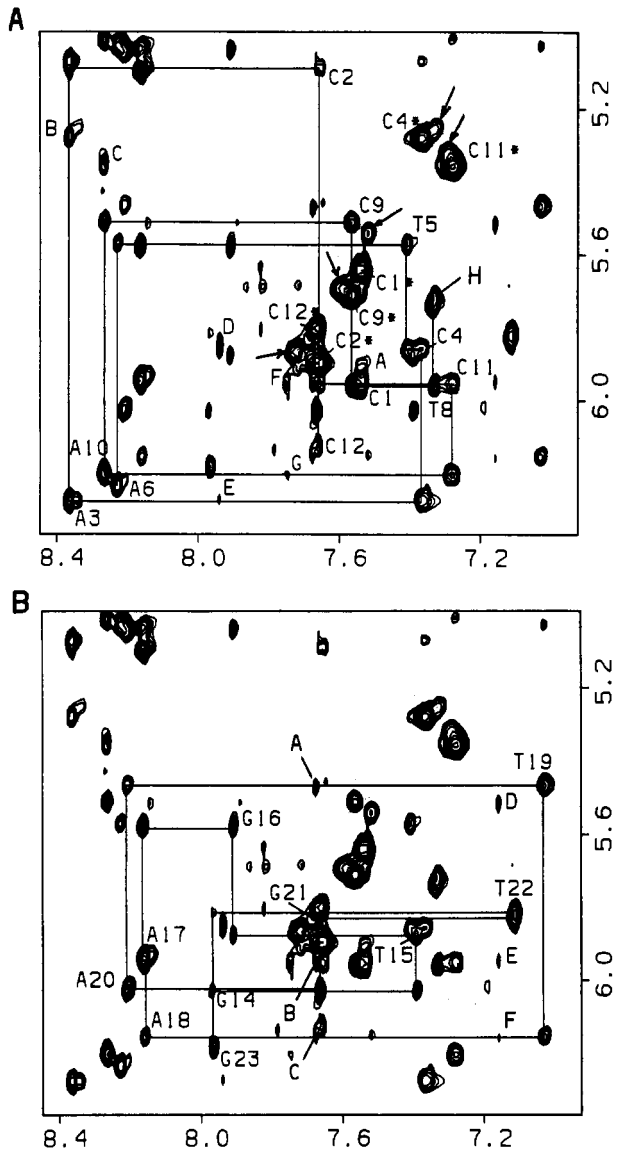

FIGURE 5: Duplicate expanded contour plots of the NOESY spectrum (250-ms mixing time) of the 8-oxo-7*H*-dG·dA 12-mer duplex in a buffer of 0.1 M NaCl and 10 mM phosphate in D_2O, pH 6.1, at 9 °C, establishing distance connectivities between the base protons (6.9–8.4 ppm) and the sugar H1′ and deoxycytidine H5 protons (5.0–6.4 ppm). (A) 8-oxo-G7 lesion containing strand traced from C1 to C12. The tracing follows connectivities between adjacent base protons through their intervening sugar H1′ protons. The deoxycytidine H5–H6 connectivities of the major conformation are designated by asterisks, while those of the minor conformation are identified by arrows. The cross peaks A–H are assigned as follows: A, C1(H6)–C2(H5); B, A3(H8)–C4(H5); C, A10(H8)–C11(H5); D, A3(H2)–C4(H1′); E, A3(H2)–A3(H1′); F, A10(H2)–C11(H1′); G, A10(H2)–A10(H1′); H, T8(H6)–oxo-G7(H1′) and T8(H6)–C9(H5). (B) A18-containing strand traced from G14 to G23. The cross peaks A–F are assigned as follows: A, A18(H2)–T19(H1′); B, A18(H2)–T8(H1′); C, A18(H2)–A18(H1′); D, A17(H2)–C9(H1′); E, A17(H2)–A17(H1′); F, A17(H2)–A18(H1′).

and deoxycytidine H5 protons (5.0–6.4 ppm) are shown in Figure 5. The observed NOE cross peaks link the base (purine H8 and pyrimidine H6) protons with their own and the 5′-flanking sugar H1′ protons (Hare et al., 1983) such that the deoxyoligonucleotide chain can be traced from dC1 to dA6 and from dT8 to dC12 for the modified strand (Figure 5A). There is a break in this tracing at 8-oxo-7*H*-dG7 because the H8 proton in this modified base has been replaced by a carbonyl oxygen atom. We can trace the deoxyoligonucleotide chain without interruption from dG14 to dG23 for the unmodified strand (Figure 5B).

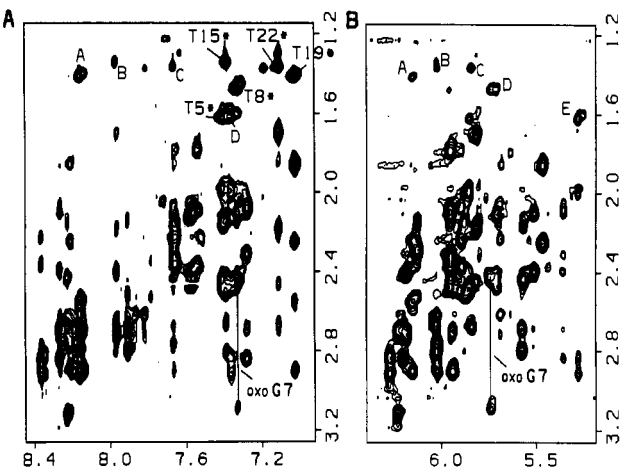

FIGURE 6: Expanded contour plots of the NOESY spectrum (250-ms mixing time) of the 8-oxo-7*H*-dG·dA 12-mer duplex in buffer of 0.1 M NaCl and 10 mM phosphate in D_2O, pH 6.1, at 9 °C. (A) NOE cross peaks establishing connectivities between the base protons (6.9–8.4 ppm) and the sugar H2′,2″ and thymidine CH_3 protons (1.2–3.2 ppm). The thymidine H6-CH_3 cross peaks are designated by asterisks. The H2′ and H2″ protons of 8-oxo-G7 at the lesion site are connected by lines. The cross peaks A–D are assigned as follows: A, A18(H8)-T19(CH_3); B, G14(H8)–T15(CH_3); C, G21(H8)–T22(CH_3); D, C4(H6)–T5(CH_3). (B) NOE cross peaks establishing connectivities between the H1′ and deoxycytidine H5 protons (5.1–6.4 ppm) and the sugar H2′,2″ and thymidine CH_3 protons (1.2–3.2 ppm). The H2′ and H2″ protons of 8-oxo-G7 at the lesion site are connected by lines. The cross peaks A–E are assigned as follows: A, A18-(H1′)–T19(CH_3); B, G14(H1′)–T15(CH_3); C, G21 (H1′)–T22(CH_3); D, A7(H1′)–T8(CH_3); E, C4(H1′)–T5(CH_3).

The NOE cross-peak intensities between the base and their own sugar H1′ protons are weak relative to the NOE cross-peak intensities between the deoxycytidine H6 and H5 protons in the short mixing time 50-ms NOESY contour plot of the 8-oxo-7*H*-dG·dA 12-mer duplex (Figure 4B). These results establish that all unmodified residues, including dA18 opposite the lesion site, adopt anti glycosidic torsion angles in the 8-oxo-7*H*-dG·dA 12-mer duplex.

Expanded NOESY contour plots that establish distance connectivities from the sugar H2′,2″ and thymidine CH_3 protons (1.2–3.2 ppm) to the base protons (6.9–8.4 ppm) and to the sugar H1′ and deoxycytidine H5 protons (5.1–6.4 ppm) in the 8-oxo-7*H*-dG·dA 12-mer duplex are plotted in Figure 6, panels A and B, respectively. We detect NOE cross peaks between the H6 proton of T8 and the sugar H2′,2″ protons of 8-oxo-7*H*-dG7 (peaks labeled oxo-G7, Figure 6A), as well as with the sugar H1′ proton of 8-oxo-7*H*-dG7 (peak H, Figure 5A), for the 8-oxo-7*H*-dG7-dT8 step in the modified strand of the 8-oxo-7*H*-dG·dA 12-mer duplex. These sugar H1′ and H2′,2″ proton assignments for 8-oxo-7*H*-dG7 are confirmed by the NOE cross peaks between the H1′ and H2′,2″ protons of 8-oxo-7*H*-dG7 (peaks labeled oxo-G7, Figure 6B) in the 8-oxo-7*H*-dG·dA 12-mer duplex.

We detect NOEs between adjacent base protons in purine H8/pyrimidine H6 (3′–5′) pyrimidine H5/CH_3 steps in the 8-oxo-7*H*-dG·dA 12-mer duplex. These include the dA3-dC4 (peak B, Figure 5A), dC4-dT5 (peak D, Figure 6A), dT8-dC9 (peak H, Figure 5A), dA10-dC11 (peak C, Figure 5A), dG14-dT15 (peak B, Figure 6A), dA18-dT19 (peak A, Figure 6A), and dG21-dT22 (peak C, Figure 6A) steps. It should be noted that the H8 of dA18 exhibits a strong NOE to the CH_3 (peak A, Figure 6A) and a weak NOE to the H6 (peak A, Figure 7A) protons of dT19, and these observations define the handedness of the dA18-dT19 step on the partner strand opposite the 8-oxo-7*H*-dG7 lesion site in the 8-oxo-7*H*-dG·dA 12-mer duplex.

Table I: Exchangeable Proton Chemical Shifts in the 8-Oxo-7*H*-dG·dA 12-mer Duplex at 9 °C[a]

	chemical shift (ppm)						
base pair	T(NH3)	G(NH1)	G(NH7)	G(NH_2-2)	C(NH_2-4)	A(H2)	A(NH_2-6)
A3·T22	13.91					7.89	
C4·G21		12.69			8.02, 6.75[b]		
T5·A20	13.68					7.14	
A6·T19	13.27					7.32	
oxo-G7·A18		10.54	12.57	6.45[c]		7.65	7.79, 5.96[d]
T8·A17	13.61					7.13	
C9·G16		12.42			8.51, 6.92[b]		
A10·T15	13.71					7.71	

[a] Buffer was 0.1 M NaCl and 10 mM phosphate in H_2O, pH 6.1. [b] Hydrogen-bonded amino proton downfield from exposed amino proton for dC4 and dC9. [c] Average resonance for oxo-dG7 amino protons. [d] Hydrogen-bonded amino proton downfield from exposed amino proton for dA18.

We also detect NOEs between thymidine CH_3 protons and the 5′-flanking sugar H1′ protons at the dC4-dT5 (peak E, Figure 6B), oxo-dG7-T8 (peak D, Figure 6B), dG14-dT15 (peak B, Figure 6B), dA18-dT19 (peak A, Figure 6B), and dG21-dT22 (peak C, Figure 6B) steps in the 8-oxo-7*H*-dG·dA 12-mer duplex. The NOEs between the CH_3 proton of T8 and the H1′ proton (peak D, Figure 6B) and H2′,2″ protons (peaks A and B, Figure 7B) of oxo-dG7 in the oxo-dG7-dT8 step define the handedness of the helix at the lesion site.

There are three deoxyadenosines in the d(A6-oxo-G7-T8)·d(A17-A18-T19) segment centered about the lesion site in the 8-oxo-7*H*-dG·dA 12-mer duplex. The NOEs between the H2 protons of deoxyadenosine in an anti orientation and nearby sugar H1′ protons can identify the handedness of the helix. The typical pattern of NOEs associated with the deoxyadenosine H2 protons are between its own sugar H1′ proton, the adjacent sugar H1′ proton in the 3′-direction on the same strand, and the adjacent sugar H1′ proton in the 5′-direction on the partner strand in a right-handed duplex. We note that the H2 proton of dA18 opposite the lesion site exhibits NOEs with the sugar H1′ protons of dA18 (peak C, Figure 5B), dT19 (peak A, Figure 5B), and dT8 (peak B, Figure 5B), while the H2 proton of dA17 exhibits NOEs with the sugar H1′ protons of dA17 (peak E, Figure 5B), dA18 (peak F, Figure 5B), and dC9 (peak D, Figure 5B). Similar patterns of NOEs are also detected for dA3 (peaks D and E, Figure 5A) and dA10 (peaks F and G, Figure 5A), which are more distant from the lesion site in the 8-oxo-7*H*-dG·dA 12-mer duplex.

Other expanded regions of the NOESY spectrum have been similarly analyzed to determine and cross-check the base and sugar H1′, H2′,2″, and H3′ proton chemical shifts in the 8-oxo-7*H*-dG·dA 12-mer duplex; these shifts are listed in Table II.

Phosphorus Spectra. We detect a partially resolved envelope of phosphorus resonance between −3.8 and −4.5 ppm in the proton-decoupled phosphorus spectrum of the 8-oxo-7*H*-dG·dA 12-mer duplex (Figure 1C). The phosphorus resonances remain unassigned at this time.

Distance Restraints and Energy Minimization. The starting model for the energy minimization studies on the 8-oxo-7*H*-dG·dA 12-mer duplex consisted of a B-form, right-handed helix. Furthermore, 8-oxo-7*H*-dG7(*syn*) was positioned opposite dA18(*anti*) without hydrogen-bonding constraints across the lesion site. We measured 151 distance constraints defined by lower and upper limits for the 8-oxo-7*H*-dG·dA 12-mer duplex from the volume integrals of resolved NOE cross peaks in NOESY spectra recorded at 50-, 80-, and 250-ms mixing times in D_2O solution. The deoxycytidine H6–H5 fixed interproton separation of 2.45 Å was used as the reference distance. The boundaries reflect the inherent uncertainties

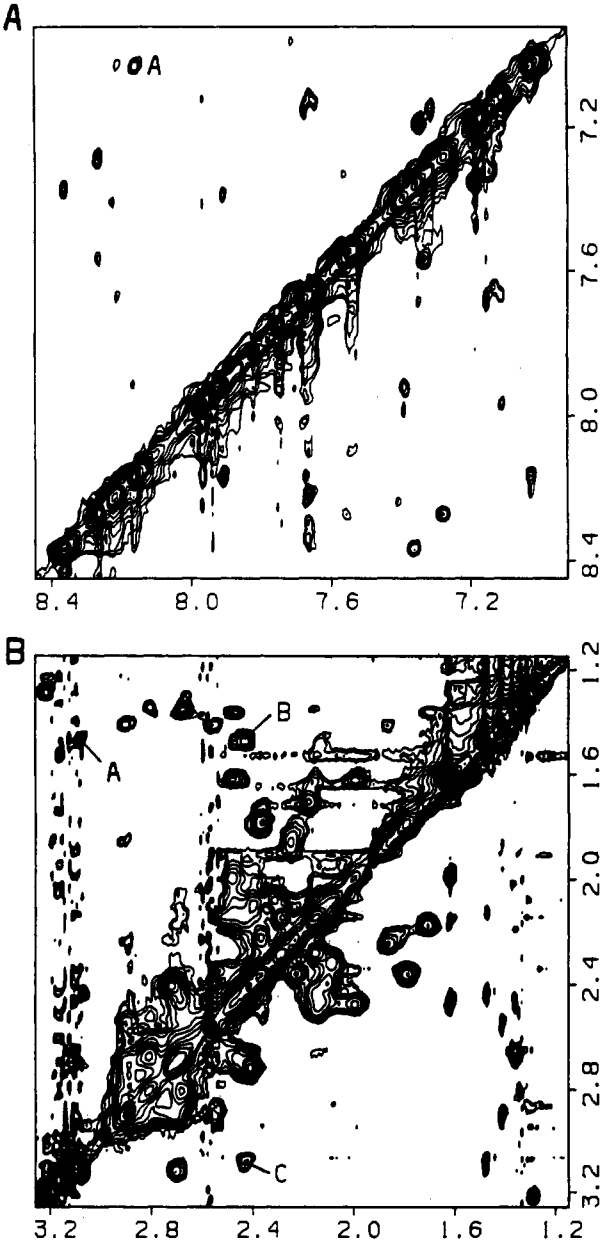

FIGURE 7: Expanded contour plots of the NOESY spectrum (250-ms mixing time) of the 8-oxo-7*H*-dG·dA 12-mer duplex in buffer of 0.1 M NaCl and 10 mM phosphate in D_2O, pH 6.1, at 9 °C. (A) NOE cross peaks in the symmetrical base proton region (6.9–8.4 ppm). The cross peak labeled A is assigned to the NOE between A18(H8) and T19(H6). (B) NOE cross peaks in the symmetrical H2′,2″ and CH_3 proton region (1.2–3.2 ppm). The cross peaks A–C are assigned as follows: A, oxo-G7(H2″)–T8(CH_3); B, oxo-G7(H2′)–T8(CH_3); C, oxo-G7(H2′)–oxo-G7(H2″).

in distance estimates using the two-spin approximation. The distance boundaries for the d(A6-oxo-G7-T8)·d(A17-A18-

Table II: Nonexchangeable Proton Chemical Shifts in the 8-Oxo-7*H*-dG·dA 12-mer Duplex at 9 °C[a]

	chemical shift (ppm)									chemical shift (ppm)							
base	H8	H2	H6	H5/CH_3	H1′	H2′	H2″	H3′	base	H8	H2	H6	H5/CH_3	H1′	H2′	H2″	H3′
C1			7.53	5.64	5.95	1.79	2.37	4.52	C12			7.67	5.80	6.13	2.16	2.33	5.09
C2			7.65	5.90	5.10	2.22	2.36	4.82	G14	7.97				6.03	2.67	2.80	
A3	8.36	7.94			6.27	2.83	2.91	5.07	T15			7.38	1.35	5.87	2.14	2.50	
C4			7.36	5.28	5.85	1.99	2.47	4.70	G16	7.90				5.57	2.68	2.80	
T5			7.40	1.61	5.57	2.15	2.43	4.87	A17	8.15	7.16			5.94	2.70	2.90	5.10
A6	8.22				6.23	2.67	3.12	5.03	A18	8.14	7.67			6.15	2.55	2.89	5.03
oxo-G7					5.72	2.47	3.09		T19			7.02	1.41	5.47	1.86	2.26	4.83
T8			7.32	1.47	5.95	2.12	2.47	4.86	A20	8.20				6.02	2.75	2.87	5.03
C9			7.56	5.71	5.51	2.09	2.39	4.85	G21	7.65				5.84	2.47	2.67	
A10	8.26	7.75			6.20	2.68	2.84	5.02	T22			7.10	1.36	5.82	1.70	2.17	4.82
C11			7.27	5.36	5.95	2.08	2.31	4.72	G23	7.96				6.18	2.40	2.72	

[a] Buffer was 0.1 M NaCl and 10 mM phosphate in D_2O, pH 6.1.

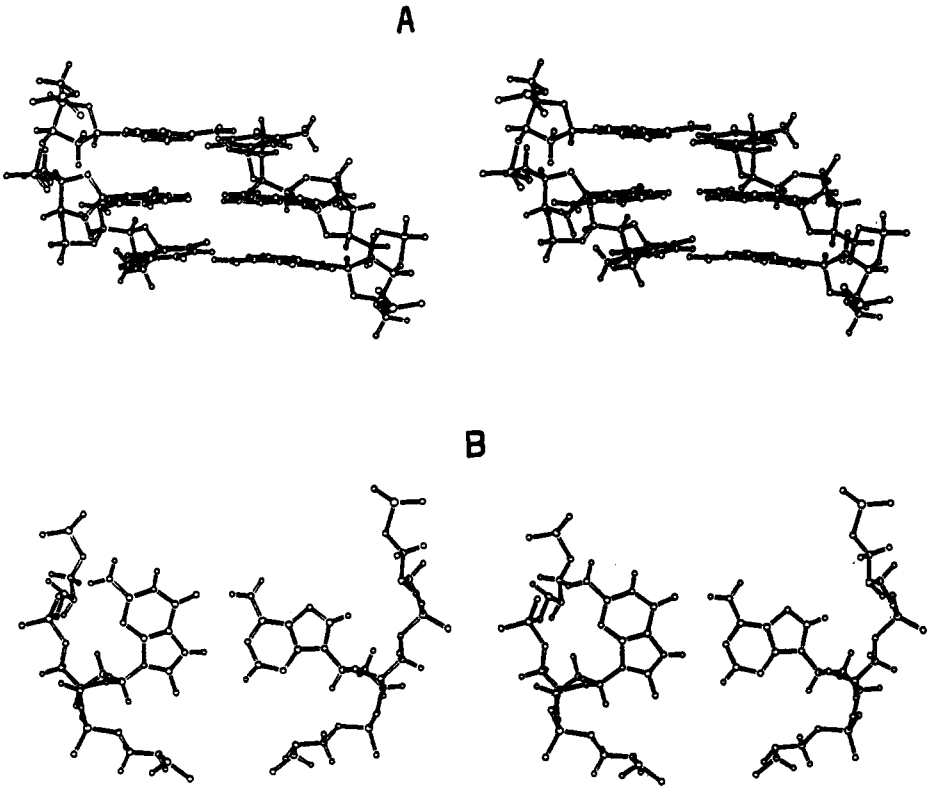

FIGURE 8: Stereopairs of (A) the d(A6-oxo-G7-T8)·d(A17-A18-T19) trinucleotide segment viewed normal to the helix axis and (B) the oxo-dG7·dA18 alignment viewed down the helix axis in the 8-oxo-7*H*-dG·dA 12-mer duplex.

T19) segment centered about the oxo-dG7·dA18 lesion site are listed in Table III. The important restraints at the lesion site are those between oxo-dG7(NH7) and dA18(H2), which is assigned limits of 2.1–3.3 Å, and between oxo-dG7(NH7) and dA18(NH_2-6), which is assigned limits of 2.5–3.7 Å. These latter NOEs, involving exchangeable protons, are based on NOE cross-peak volume integrals measured for the NOESY spectrum at a mixing time of 120 ms in H_2O solution with the 2.7-Å thymidine imino to deoxyadenosine H2 separation within a Watson–Crick dA·dT pair as the reference distance.

The energy-minimized structure establishes that the oxo-dG7(*syn*)·dA18(*anti*) lesion site can be accommodated readily within a right-handed helix without disruption of flanking base pairs. A stereo pair of the d(A6-oxo-G7-T8)·d(A17-A18-T19) trinucleotide segment of this proposed structure viewed normal to the helical axis is plotted in Figure 8A. The oxo-dG7-(*syn*)·dA18(*anti*) alignment viewed down the helix axis of the energy-minimized structure is plotted in Figure 8B and appears to be stabilized by NH7(oxo-dG7)·N1(dA18) and O6(oxo-dG7)·NH_2-6(dA18) hydrogen bonds as shown schematically in **3**. The interproton distances for the d(A6-oxo-G7-T8)·d-(A17-A18-T19) segment measured from the energy-minimized structure of the 8-oxo-7*H*-dG·dA 12-mer duplex are listed in Table IV.

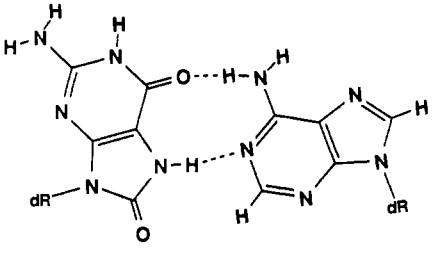

3

Discussion

Minor Component. The two-dimensional spectra of the 8-oxo-7*H*-dG·dA 12-mer duplex clearly demonstrates that the NOE for each deoxycytidine H6–H5 pair exhibits major

Table III: Proton–Proton Distance Constraints in the d(A6-oxo-G7-T8)·d(A17-A18-T19) Segment of the 8-Oxo-7*H*-dG·dA 12-mer Duplex[a]

	Intraresidue Constraints on the Same Strand				
	H6/H8–H1′	H6/H8–H2′	H6/H8–H2″	H1′–H2′	H1′–H2″
A6	3.3–4.7[b]	[c]	2.6–4.0[b]	[c]	2.1–3.5[b]
oxo-G7				[c]	2.7–4.1[b]
T8	3.3–4.7[b]	2.0–3.4[b]	[c]	[c]	2.0–3.4[b]
A17	[c]	[c]	[c]	[c]	2.1–3.5[b]
A18	3.7–5.1[b]	2.0–3.4[b]	[c]	2.4–4.2[b]	2.1–3.5[b]
T19	3.0–4.4[b]	2.0–3.4[b]	2.5–3.9[b]	2.4–3.8[b]	2.0–3.3[b]

	Interresidue Constraints on the Same Strand			
	H1′–H6/H8	H2′–H6/H8	H6/H8–CH_3	H1′–CH_3
T5–A6	2.7–4.5[d]	3.3–4.7[b]		
A6–oxo-G7				
oxo-G7–T8	[c]	[c]		2.7–5.0[d]
T8–C9	[c]	[c]		
G16–A17	3.1–4.5[b]	[c]		
A17–A18	[c]	[c]		
A18–T19	3.4–4.8[b]	3.0–4.4[b]	2.2–4.5[b]	2.7–5.0[d]
T19–A20	3.3–4.7[b]	2.7–4.1[b]		

	Interresidue Constraints on Partner Strands		
	A18(H2)	A18(NH_2-6)	A18(NH_2-6)
oxo-G7(NH7)	2.1–3.3	2.5–3.7	3.0–5.0

[a] All constraints are given in angstroms. [b] 50- and 80-ms data in D_2O. [c] Overlap. [d] 250-ms data in D_2O.

(designated by asterisks) and minor (designated by arrows) cross peaks in 50-ms (Figure 4B) and 250-ms (Figure 5A) mixing time NOESY contour plots. We estimate that the minor component constitutes less than 15% of the mixture and that the exchange between the components is slow on the NMR time scale. The NOE cross peaks for the minor component between proton pairs other than those between H6 and H5 of deoxycytidines are generally too weak to detect and hence the analysis of the two-dimensional spectra of the major component could be undertaken without undue complications.

We can establish that the major component corresponds to the 6,8-dioxo tautomer at the lesion site and must assume at this time that the minor component corresponds to one of the other possible keto–enol tautomers (Culp et al., 1989). Alternatively, the minor component could reflect a pairing arrangement different from the 8-oxo-7*H*-dG7(*syn*)·dA18(*anti*) alignment established for the major component in the 8-oxo-7*H*-dG·dA 12-mer duplex. The purity of the synthesized protected 8-oxo-7*H*-dG, as well as the dodecamer strand following incorporation of 8-oxo-7*H*-dG, was established unequivocally (see Experimental Procedures), ruling out sample heterogeneity as a source of the minor component in the 8-oxo-7*H*-dG·dA 12-mer duplex.

Spectral Assignments of Major Component. The NOESY data sets of the 8-oxo-7*H*-dG·dA 12-mer duplex in H_2O (Figure 2) and D_2O (Figure 4A) were of sufficient quality to permit assignment of the exchangeable imino and amino protons, as well as the nonexchangeable base and sugar H1′, H2′,2″, and H3′ protons, including those at the oxo-dG7·dA18 lesion site. These assignments, listed in Tables I and II, were considerably aided by the fact that the majority of the NOEs corresponded to those expected for regular right-handed helices in segments flanking and centered about the lesion site.

Our ability to assign the NH1, NH7, and NH_2-2 base protons of 8-oxo-7*H*-dG7 and the H8, H2, and NH_2-6 base protons of dA18, as well as the H1′, H2′,2″, and H3′ protons of both residues has provided the necessary markers to monitor the oxo-dG7·dA18 lesion site. Further, the exchangeable and nonexchangeable protons of adjacent dA6·dT19 and dT8·dA17 base pairs are also well-resolved and have been assigned so that the NMR parameters should provide structural insights into the d(A6-oxo-G7-T8)·d(A17-A18-T19) segment centered about the lesion site.

General Structural Features of Duplex. The observed pattern of NOEs between thymidine imino protons and deoxyadenosine H2 protons (peaks A–E, Figure 2) establishes the formation of Watson–Crick dA·dT pairs including dA6·T19 and dT8·dA17, which flank the lesion site in the 8-oxo-7*H*-dG·dA 12-mer duplex. Similarly, the observed NOEs between deoxyguanosine imino protons and deoxycytidine amino protons (peaks J,K and L,M, Figure 2) establish Watson–Crick alignment at dC4·dG21 and dC9·dG16 pairs in the helix.

The pattern of the NOE cross peaks between protons on adjacent residues defines the handedness of the helix. For right-handed duplexes, NOE patterns are predicted between the base protons and their 5′-flanking but not 3′-flanking sugar protons, as well as between adjacent base protons in purine (3′–5′) pyrimidine but not pyrimidine (3′–5′) purine steps (Hare et al., 1983). The directionality of the distance connectivities outlined in Figures 5–7 and presented under Results is consistent with a right-handed helix with stacked bases for the 8-oxo-7*H*-dG·dA 12-mer duplex. The weak signal intensity of the base protons to their own sugar H1′ protons in the short mixing time NOESY data sets (Figure 4B) requires that the glycosidic torsion angles be in the anti range (Patel et al., 1982) for all unmodified residues in the 8-oxo-7*H*-dG·dA 12-mer duplex.

8-Oxo-7H-dG7(syn) at the Lesion Site. The 6,8-dioxo tautomer of 8-oxo-7*H*-dG7 has imino protons at NH1 and NH7 and amino protons at the NH_2-2 position. The averaged 6.45 ppm amino protons exhibit an NOE to the 10.54 ppm but not the 12.57 ppm imino protons (Figures 2 and 3B), permitting assignment of the former to the NH1 and the latter to the NH7 protons on the 8-oxo-7*H*-dG7 ring in the 8-oxo-7*H*-dG·dA 12-mer duplex. We can also conclude that the NH1 proton is not hydrogen-bonded due to its upfield chemical shift of 10.54 ppm, whereas NH7 is hydrogen-bonded due to its downfield chemical shift of 12.57 ppm. The data require that 8-oxo-7*H*-dG7 adopt a syn orientation about the glycosidic bond and that the Hoogsteen edge (with its NH7 proton) be directed toward the partner strand and, thereby, form a hydrogen bond with an acceptor group on A18.

The observed NOEs from the 12.57 ppm NH7 imino proton of 8-oxo-7*H*-dG7(*syn*) to the thymidine imino protons of flanking Watson–Crick dA6·dT19 and dT8·dA17 pairs (Figure

Table IV: Proton–Proton Distances in the d(A6-oxo-G7-T8)·d(A17-A18-T19) Segment of the 8-Oxo-7*H*-dG·dA 12-mer Duplex from the Energy-Minimized Model[a]

	H6/H8–H1′	H6/H8–H2′	H6/H8–H2″	H1′–H2′	H1′–H2″
	Intraresidue Distances on the Same Strand				
A6	3.8	2.2	3.2	3.0	2.5
oxo-G7				3.0	2.5
T8	3.7	2.2	3.4	3.0	2.5
A17	3.8	2.1	3.3	3.0	2.5
A18	3.9	2.3	3.5	3.0	2.5
T19	3.7	2.1	3.3	3.0	2.5

	H1′–H6/H8	H2′–H6/H8	H6/H8–CH_3	H1′–CH_3
	Interresidue Distances on the Same Strand			
T5–A6	3.4	4.6		
A6–oxo-G7				
oxo-G7–T8	3.2	3.8		4.8
T8–C9	2.9	4.1		
G16–A17	3.4	5.0		
A17–A18	2.9	4.4		
A18–T19	3.3	4.4	4.1	4.8
T19–A20	3.3	4.5		

	A18(H2)	A18(NH_2-6)	A18(NH_2-6)	A6(H2)
	Interresidue Distances on Partner Strands			
oxo-G7(NH7)	2.6	3.4	4.8	3.0

step	proton pair	distance
	Interresidue Distances in d(A6-oxo-G7-T8) Segment	
A6–oxo-G7	A6(H8)–oxo-G7(NH1)	4.1
oxo-G7–T8	oxo-G7(H1′)–T8(H6)	3.2
oxo-G7–T8	oxo-G7(H2″)–T8(H6)	2.3
oxo-G7–T8	oxo-G7(H2′)–T8(H6)	3.8
oxo-G7–T8	oxo-G7(H1′)–T8(CH_3)	4.8
oxo-G7–T8	oxo-G7(H2″)–T8(CH_3)	3.1
oxo-G7–T8	oxo-G7(H2′)–T8(CH_3)	3.7

step	proton pair	distance
	Interresidue Distances in d(A17–A18–T9) Segment	
A18–T19	A18(H8)–T19(H6)	5.0
A18–T19	A18(H8)–T19(CH_3)	4.1

residue	proton pair	distance
	Distances Involving H2 Protons of dA17 and dA18	
A17	A17(H2)–A17(H1′)	4.6
A17	A17(H2)–A18(H1′)	4.0
A17	A17(H2)–C9(H1′)	3.3
A18	A18(H2)–A18(H1′)	4.5
A18	A18(H2)–T19(H1′)	3.8
A18	A18(H2)–T8(H1′)	3.3

residue	proton pair	distance
	Inter-Base-Pair Distances Involving H2 protons of dA18	
A18	A18(H2)–T8(NH3)	3.2
A18	A18(H2)–T19(NH3)	3.8

[a] All distances are given in angstroms.

3C) are consistent with the NH7 proton pointing toward the helix axis and stacking between flanking dA·dT pairs. Similarly, the observed NOE between the 10.54 ppm NH1 imino proton of 8-oxo-7*H*-dG7(*syn*) and the major-groove H8 proton of dA6(*anti*) (Figure 3B) is consistent with the NH1 proton being directed outward from the helix toward the major groove.

The observed NOEs between the CH_3-5 of T8 and the sugar H1′ (peak D, Figure 6B) and H2′,2″ (peaks A and B, Figure 7B) protons of 8-oxo-7*H*-dG7 establishes that the oxo-dG7-dT8 step is part of a right-handed helical segment in the 8-oxo-7*H*-dG·dA 12-mer duplex.

dA18(anti) at the Lesion Site. Several lines of evidence establish that dA18 opposite the lesion site adopts an anti glycosidic torsion angle and is stacked into a right-handed helical segment in the 8-oxo-7*H*-dG·dA 12-mer duplex. This includes the observation of a very weak NOE between the H8 proton of dA18 and its own sugar H1′ proton at short mixing times (Figure 4B), a cross-strand NOE between the H2 proton of dA18 and the H1′ proton of dT8 (peak B, Figure 5B), and NOEs between the CH_3 of dT19 and the H8 (peak A, Figure 6A), H1′ (peak A, Figure 6B), and H2′,2″ (Figure 7B) protons of dA18 in the dA18-dT19 step. We also detect NOEs between the H2 protons of dA18 at the lesion site and the imino protons of Watson–Crick dT8·dA17 and dA6·dT19 pairs (peaks H and I, Figure 2), which flank the lesion site so that the H2 proton of dA18 is directed toward the helix axis consistent with an anti orientation.

Oxo-dG7(syn)·dA18(anti) Alignment. The observed NOEs from the NH7 proton of 8-oxo-7*H*-dG7 to the H2 and NH_2-6 protons of dA18 (Figures 2 and 3C) provide the strongest evidence for alignment of the Hoogsteen edge of 8-oxo-7*H*-dG7(*syn*) with the Watson–Crick edge of dA18(*anti*) at the lesion site in the 8-oxo-7*H*-dG·dA 12-mer duplex. These data also require that NH7 of 8-oxo-7*H*-dG7(*syn*) be positioned opposite N1 (which is between H2 and NH_2-6) of dA18 and be hydrogen-bonded to it (the 12.57 ppm downfield chemical shift for NH7 is characteristic of an imino proton hydrogen-bonded to a ring nitrogen). This alignment can be stabilized by a second hydrogen bond between the O6 carbonyl of 8-oxo-7*H*-dG7(*syn*) and the NH_2-6 proton of dA18(*anti*), as shown schematically in **3**. The NH_2-6 protons of dA18 are separated by 1.83 ppm, consistent with the downfield amino proton (7.79 ppm) participating in a hydrogen bond relative to the upfield amino proton (5.96 ppm), which would not be expected to hydrogen bond and thus would be exposed to solvent.

The 8-oxo-7*H*-dG7(*syn*)·dA18(*anti*) alignment (**3**) directs the O8 carbonyl group of 8-oxo-7*H*-dG7(*syn*) toward the minor groove, in which it is readily accommodated. The non-hydrogen-bonded 10.45 ppm NH1 imino and 6.45 ppm NH_2-6 averaged amino protons of 8-oxo-7*H*-dG7(*syn*) are directed toward the major groove, and their chemical shifts are similar to those reported earlier for the dG(*syn*)·protonated dA(*anti*) mismatch (Gao & Patel, 1988) and for the aminofluorene C8-modified dG(*syn*)·dA(*anti*) lesion site (Norman et al., 1989).

d(A6-oxo-G7-T8)·d(A17-A18-T19) Segment. The interproton distances in the central trinucleotide segment in the energy-minimized model of the 8-oxo-7*H*-dG·dA 12-mer duplex (Table IV) can be compared with the corresponding experimental distance constraints listed in Table III and reflected in the NOE cross peaks in one- and two-dimensional NMR spectra. The tabulated distances between base and sugar protons on the same residue and between adjacent residues in the energy-minimized structure are consistent with a regular right-handed DNA helix at the central trinucleotide segment, which includes the lesion site. Several interproton distances of <5 Å are observed between 8-oxo-7*H*-dG7 exchangeable protons and protons on adjacent residues in the energy-minimized model that are a consequence of the syn orientation of the 8-oxo-7*H*-dG7 residue. Experimentally, we detect NOE cross peaks between these proton pairs in the 8-oxo-7*H*-dG·dA 12-mer duplex in support of the proposed oxo-dG7(*syn*)·dA18(*anti*) alignment at the lesion site. The critical distances are 2.6 Å for oxo-dG7(NH7)–dA18(H2) and 3.4 Å for oxo-dG7(NH7)–dA18(NH_2-6) across the lesion site, as well as 3.0 Å for oxo-dG7(NH7)–dA6(H2), 4.1 Å for oxo-dG7(NH1)–dA6(H8), 4.1 Å for dA18(H8)–dT19(CH_3), 3.3 Å for dA18(H2)–dT8(H1′), 3.2 Å for dA18(H2)–dT8(NH3), and 3.8 Å for dA18(H2)–dT19(NH3). These NOEs reflect the positioning of the NH7 of 8-oxo-7*H*-dG7 and the H2 of dA18 near the helix axis in the interior of the duplex

and the NH1 of 8-oxo-7*H*-dG7 in the major groove pointing toward solvent.

C8-Substituted Deoxyguanosine Lesions. The present study on the 8-oxo-7*H*-dG·dA lesion site represents the second structural characterization of a C8-modified dG positioned opposite dA at the DNA oligomer duplex level. The earlier NMR study reported on an aminofluorene (AF) adduct covalently attached to the C8 position of dG and the characterization of the resulting AF-dG·dA lesion site (Norman et al., 1989). The NMR studies establish 8-oxo-7*H*-dG(*syn*)·dA(*anti*) and AF-dG(*syn*)·dA(*anti*) alignments such that in each case the substituent at the C8 position of the modified dG residue is readily accommodated in the minor groove.

Biological Implications. Nishimura and his colleagues first reported that dG is hydroxylated when DNA is exposed to ionizing radiation or to chemical agents that generate free radicals derived from oxygen (Kasai & Nishimura, 1984a–c; Kasai et al., 1984, 1986). Introducing an oxygen atom at the C8 position of dG alters the electronic properties of dG, rendering it capable of pairing with bases other than dC (Aida & Nishimura, 1987). In their monomeric form, 8-substituted deoxypurines assume the *syn* conformation (Uesugi & Ikehara, 1977). As shown in the present paper, 8-oxo-7*H*-dG(*syn*) also forms a stable structure in duplex DNA when paired with dA(*anti*). The relative stability of this base pair may account for the relatively high efficiency with which it is extended by DNA polymerase (Shibutani et al., 1991).

Factors other than base pairing (e.g., binding to DNA polymerase and accessory proteins) may contribute to the conformation of template DNA in the replication complex. Unless removed during proofreading, pairing of dA to 8-oxo-7*H*-dG results in miscoding, and it has been demonstrated that 8-oxo-7*H*-dG directs incorporation of dA as well as dC opposite the lesion on primed templates in reactions catalyzed by DNA polymerases (Shibutani et al., 1991). In addition, dG → dT transversions, targeted to the site of the lesion, were observed when M13 DNA (Wood et al., 1990) or gapped plasmids (Moriya et al., 1991) containing 8-oxo-7*H*-dG were used for studies of site-specific mutagenesis in *Escherichia coli*.

Acknowledgments

The XPLOR Version 1.5 program was kindly provided by Dr. Axel Brunger, Department of Biochemistry and Molecular Biophysics, Yale University. We thank Mr. Robert Rieger for preparing the modified oligodeoxynucleotides used in these experiments.

Registry No. 8-Oxo-7H-dG·dA 12-mer, 130669-63-5.

References

Aida, M., & Nishimura, S. (1987) *Mutat. Res. 192*, 83–89.
Bodepudi, V., Iden, C. R., & Johnson, F. (1991) *Nucleosides Nucleotides* (in press).
Breimer, L. H. (1988) *Br. J. Cancer 57*, 6–18.
Brunger, A. (1988) XPLOR Version 1.5, User Manual, Yale University.
Cerutti, P. A. (1985) *Science 227*, 335.
Culp, S. J., Cho, B. P., Kadlubar, F. F., & Evans, F. E. (1989) *Chem. Res. Toxicol. 2*, 416-422.
DiGuiseppi, J., & Fridovich, I. (1984) *CRC Crit. Rev. Toxicol. 12*, 315.
Dizdaroglu, M. (1985) *Biochemistry 24*, 4476-4481.
Gao, X., & Patel, D. J. (1988) *J. Am. Chem. Soc. 110*, 5178-5182.
Hare, D. R., Wemmer, D. E., Chou, S. H., Drobny, G., & Reid, B. R. (1983) *J. Mol. Biol. 171*, 319-336.
Hutterman, J., Kohnlein, W., Teoule, R., & Bertinchamps, A. J., Eds. (1978) *Effect of Ionizing Radiation on DNA*, Springer-Verlag, New York.
Kasai, H., & Nishimura, S. (1984a) *Nucleic Acids Res. 12*, 2137-2145.
Kasai, H., & Nishimura, S. (1984b) *Gann 75*, 565-566.
Kasai, H., & Nishimura, S. (1984c) *Gann 75*, 841-844.
Kasai, H., Tanooka, H., & Nishimura, S. (1984) *Gann 75*, 1037–1039.
Kasai, H., Crain, P. F., Kuchino, Y., Nishimura, S., Ootsuyama, A., & Tanooka, H. (1986) *Carcinogenesis 7*, 1849-1851.
Kouchakdjian, M., Marinelli, E., Gao, X., Johnson, F., Grollman, A., & Patel, D. J. (1989) *Biochemistry 28*, 5647-5657.
Kouchakdjian, M., Eisenberg, M., Live, D., Marinelli, E., Grollman, A. P., & Patel, D. J. (1990) *Biochemistry 29*, 4456-4465.
Kuchino, Y., Mori, F., Kasai, H., Inoue, H., Iwai, S., Miura, K., Ohtsuka, E., & Nishimura, S. (1987) *Nature 327*, 77.
Lin, T. S., Chen, T.-C., Ishiguro, K., & Sartorelli, A. C. (1985) *J. Med. Chem. 28*, 1194.
Maniatis, T., Fritsch, E. F., & Sambrook, J. (1982) *Molecular Cloning: A Laboratory Manual*, Cold Spring Harbor Laboratory, Cold Spring Harbor, NY.
Moriya, M., Ou, C., Bodepudi, V., Johnson, F., Takeshita, M., & Grollman, A. P. (1991) *Mutat. Res.* (in press).
Norman, D., Abuaf, P., Hingerty, B. E., Live, D., Grunberger, D., Broyde, S., & Patel, D. J. (1989) *Biochemistry 28*, 7462-7476.
Patel, D. J. Kozlowski, S. A., Nordheim, A., & Rich, A. (1982) *Proc. Natl. Acad. Sci. U.S.A. 79*, 1413-1417.
Shibutani, S., Gentles, R. G., Iden, C. R., & Johnson, F. (1990) *J. Am. Chem. Soc. 112*, 5667.
Shibutani, S., Takeshita, M., & Grollman, A. P. (1991) *Nature* (in press).
Takeshita, M., Chang, C.-N., Johnson, F., Will, S., & Grollman, A. P. (1987) *J. Biol. Chem. 262*, 10171-10179.
Ti, G. S., Gaffney, B. L., & Jones, R. A. (1982) *J. Am. Chem. Soc. 104*, 1316.
Uesugi, J., & Ikehara, M. (1977) *J. Am. Chem. Soc. 99*, 3250–3253.
Ward, J. F. (1988) *Prog. Nucleic Acid Res. Mol. Biol. 35*, 95-125.
Wood, M. L., Dizdaroglu, M., Gajewski, E., & Essigmann, J. M. (1990) *Biochemistry 29*, 7024–7032.